ISBN: 978-3-95450-204-2 ISSN: 2673-5350 doi:10.18429/JACoW-IBIC2019-MOPP014

DESIGN OF THE ESS MEBT FARADAY CUP

A. R. Páramo†, I. Bustinduy, D. de Cos[1], C. de la Cruz[2], I. Mazkiaran, R. Miracoli, V. Toyos, S. Varnasseri, Consorcio ESS-Bilbao, Zamudio, Spain
E. Donegani, J. P. Martins, European Spallation Source ERIC, Lund, Sweden
[1] also at Departamento de Física Aplicada II UPV/EHU, Vitoria, Spain
[2] also at Centro Nacional del Hidrógeno CNH2, Puertollano, Spain

Abstract

The European Spallation Source (ESS) is currently under construction and the Medium Energy Beam Transfer (MEBT) is developed by ESS-Bilbao as an in-kind contribution. In the MEBT a set of diagnostics is included for beam characterization, among them the MEBT Faraday Cup is used to measure beam current and as a beam stopper for the commissioning modes. The main challenges for the design and manufacturing of the Faraday Cup (FC) are the high irradiation loads and the necessity of a compact design due to the space constraints in the MEBT. We describe the design of the FC, characterized by a graphite collector, required to withstand irradiation, and a repeller for suppression of secondary electrons. For the operation of the Faraday Cup acquisition electronics and control system are developed, all systems have been integrated in the ESS-Bilbao ECR ion source to test operation under beam conditions. In this work, we discuss the design of the Faraday Cup, the results of the tests and how they agree with the expected performance of the Faraday Cup.

INTRODUCTION

The European Spallation Source (ESS) is currently under construction in Lund, Sweden [1,2]. The ESS linear accelerator (Linac) delivers 2 GeV protons to the tungsten target for neutron production. In the normal conducting Linac, the Medium Energy Beam Transport line (MEBT) matches, focuses and characterizes the proton beam before acceleration in the normal conduction DTLs and the superconducting cavities. To characterize the beam, the MEBT (see Figure 1) includes different kinds of diagnostics: Wire Scanners (WS), Beam Position Monitors (BPM), Beam Current Transformers (BCM), Collimation Scrapers (SC), a Slit and Grid Emittance Measurement Unit (EMU) and a Faraday Cup (FC).

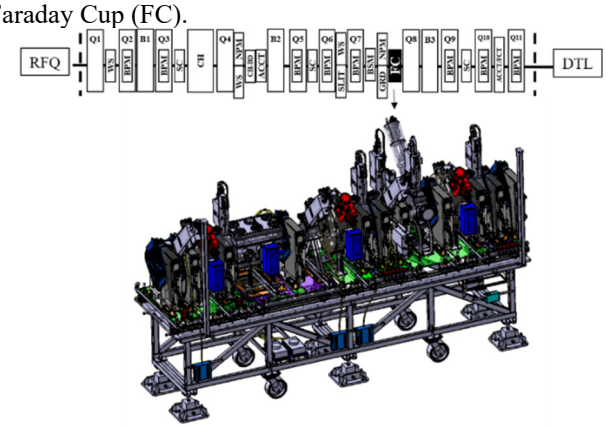

Figure 1: Scheme showing the ESS MEBT.

The MEBT will operate with a proton beam of 3.63 MeV and 62.5 mA peak current, and the FC will be used to measure the beam current and as a beam stopper during the MEBT commissioning.

In the Faraday Cup, the beam irradiates the collector and leads to high energy deposition during the pulse duration. As a result of the high currents (62.5 mA) and proton energies (3.63 MeV), the beam power is ~230 kW, that combined with a beam size of $\sigma_x \sim \sigma_y \sim 2.5$ mm [3], makes the requirements of the ESS MEBT Faraday Cup specially challenging.

Due to irradiation constraints, the operation of the FC is designed only for ESS commissioning modes: Fast tuning with pulses of 5 µs at frequencies of 14 Hz and Slow Tuning with 50 µs pulses at 1 Hz. The main operational parameters of the Faraday Cup operation are summarized in Table 1.

Table 1: Operational Parameters in the MEBT FC

Parameter	Value
Proton Energy	3.63 MeV
Intensity	62.5 mA
Beam Power	230 kW
Fast Tuning Mode	5 µs - 14 Hz
Slow Tuning Mode	50 µs - 1 Hz
Beam Size	$\sigma_x \sim \sigma_y \sim 2.5$ mm
Irradiation Power	5800 MW/m^2

The ESS MEBT Faraday Cup has an aperture of Φ48 mm, a total length of just 40 mm and is designed with a modular approach that allows for maintenance and replacement of its components, specially the collector which may undergo irradiation effects. A graphite collector is chosen due to its good capabilities to withstand the thermal shock of irradiation, selecting a high conductivity isostatic fine grain graphite SGL R7550, and with an indented profile similar to SNS DTL Faraday Cup [4] to reduce irradiation flux. A copper repeller is included for secondary electrons suppression operating at a nominal voltage of -1000 V and a refrigerated steel body allows for heat removal. The design of the Faraday Cup has been done by ESS-Bilbao and the manufacturing and assembly by the company Pantechnik. In Figure 2, we show the FC with its collector, repeller, insulators, refrigerated body and conduits.

For the operation of the Faraday Cup, integration with the electronics and control system is required. The different systems have been integrated and tested in the Bilbao ECR

ISBN: 978-3-95450-204-2 ISSN: 2673-5350 doi:10.18429/JACoW-IBIC2019-MOPP014

ion source and we analyse the results and its agreement with the expected performance of the FC.

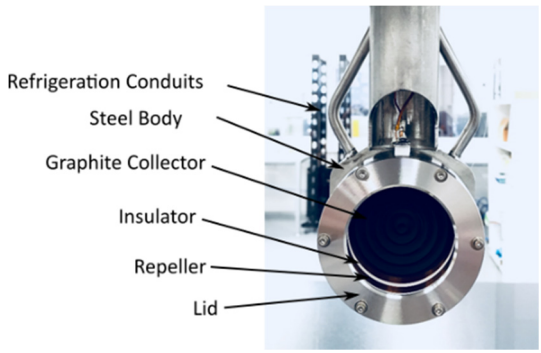

Figure 2: Faraday Cup head with its main components.

FC IRRADIATION

Due to the high power beam (3.63 MeV, 62.5 mA) and reduced beam size (σ_x~σ_y~2.5 mm), high temperature and stresses will appear in the graphite collector during irradiation. Basically, during irradiation the beam will be deposited in the first microns of the collector, leading to a temperature increase that induces a surface expansion and the appearance of compressive stresses.

The deposited power (P) depends on the beam current (I_0), stopping power (S), beam size (σ) and irradiation angle (ϕ) as:

$$P(x,y,z) = \frac{I_0 \cdot S(z,\phi)}{2\pi\sigma_x\sigma_y/\cos(\phi)} \cdot e^{-\frac{x^2}{2\sigma_x^2}} \cdot e^{-\frac{x^2}{2\sigma_y^2}} \quad (1)$$

In order to estimate the beam stopping power we use MCNPX [5] and from the energy deposition we estimate the thermomechanical effects of irradiation using an Ansys FEM model [6]. For which we use a 1D elastic model under plane strain conditions. The 1D approximation can be used since the beam is deposited in 10-150 µm depths, while the beam size is σ~2.5 mm and axial effects are dominant over the radial contribution. Finally, we compared the 1D model to 3D models, obtaining similar results.

We study the thermomechanical response to irradiation for different materials: Graphite SGL 7550 [7], TZM [8], Tungsten, Copper and Stainless Steel [9]. For 3.63 MeV proton irradiation on tungsten, TZM or Steel, the beam is deposited in the first 50 µm with stopping powers over ~1500 MeV/cm. In the case of graphite, the penetration depth is larger, up to ~130 µm with maximum stopping powers of ~750 MeV/cm.

In Figure 3 a) we show the temperature transient in the collector as function of the pulse duration. For pulses of 50 µs a temperature increase of ~800ºC takes place in graphite or copper and over 1000 ºC for W, TZM or steel. To compensate the thermal expansion, compression stresses appear at the irradiated zone. In general, we aim for a design where the maximum stress is below 2/3 of the material limit. For graphite the compressive strength is 130 MPa, for tungsten and TZM is ~1 GPa, while for strengthen drawn copper or steel is ~500 MPa. In Figure 3 b) we show the ratio of the compressive stress from irradiation (σ) to the material limit (σ_{Lim}). Studying the different materials, tungsten or TZM would undergo plastic effects in irradiation times of 5-10 µs, copper in ~3 µs and for steel in less ~1 µs, which is much shorter than the required pulse duration of 50 µs for the MEBT commissioning (see Table 1). In the case of graphite, longer pulses can be withstood, and stresses of ~2/3·$\sigma_{\mathrm{Lim.}}$ are attained at ~80 µs for perpendicular irradiation and over 100 µs for 60º inclined irradiation (dashed line).

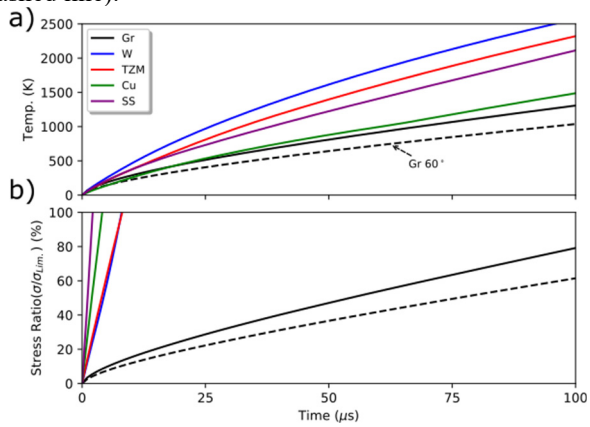

Figure 3: Thermomechanical behavior of different materials under irradiation under the conditions expected in the ESS MEBT FC (3.63 MeV, 62.5 mA, σ=2.5 mm).

Under repetitive irradiation the graphite collector is heated with an average heat load of ~16 W (see Table 1). In the steady state the collector temperature would be of ~90ºC, see Figure 4, much lower than due to the pulse transient which can be up to ~800ºC. The heat load is removed through refrigeration in the FC steel body by conduits of ϕ 4 mm and a water flow of ~2 l/min. An alumina insulator is placed between the graphite collector and the cooled steel body, allowing for electrical insulation, while having an acceptable thermal conductivity. All the components are pressed together using a closing lid that exert contact pressure of ~1MPa, than can lead to contact conductance of ~1000 W/m^{2}K, although exact values are highly dependant on particular contact conditions (rugosity, hardness) [10].

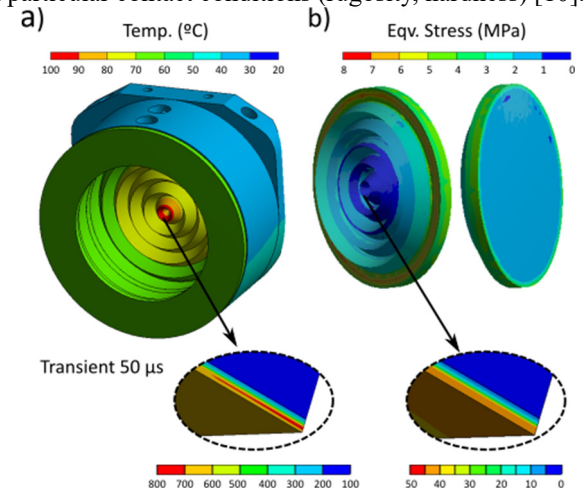

Figure 4: a) Temperature in the steady state for the MEBT FC and b) equivalent (Von Mises) stresses in the graphite collector.

ISBN: 978-3-95450-204-2 ISSN: 2673-5350 doi:10.18429/JACoW-IBIC2019-MOPP014

The previous analysis shows that graphite is an adequate material for withstanding the thermal shock of irradiation. However, over continuous irradiation other detrimental effects such a surface erosion, cracks or blistering may appear over beam deposition. Overall, a detailed estimation of the irradiation effects and how they affect to the operation of the FC can only be developed through on-site experimentation and continuous operation in the ESS MEBT. The modular design of the Faraday Cup is specially intended for collector replacement in case long term irradiation affects the integrity of the graphite.

SE SUPPRESSION

Secondary Electron (SE) yield takes place in three phases, *i)* electron production from proton irradiation, *ii)* electron transport in the material, *iii)* surface scape, which is a threshold process [11]. The emission of secondary electrons is mostly a surface effect. While 3.6 MeV protons have penetration depths of ~100 μm, the created secondary electrons with energies up to ~100-200 eV have mean free paths of ~100 nm. Therefore, only effects that take place in the graphite surface (~100 nm depth) are relevant for the estimation of secondary electron yields.

For the secondary electron emission we use the spectrum reported for 1 MeV proton irradiation on carbon foils by Drexler et al [12]. In the spectrum, there is a peak at ~3 eV, decreasing one order of magnitude for energies >20 eV, and with a small fraction of secondary electrons generated up to ~100-200 eV. For the angular emission probability, we assume it to be dependent on the cosine of the secondary electron emission, cos(θ), where θ is the angle between the emitted electron direction and the irradiated surface. The secondary electron source footprint is defined by the proton beam gaussian profile of σ_x=σ_y=2.5 mm (see Table 1).

The electrostatic field in the FC is calculated using Ansys [6]. In the model, we include the FC geometry using an axisymmetric model and set the repeller voltage to V_{rep}=-1000 V and the collector, lid and external boundaries to V_{ground}=0 V. Finally, the tracing of secondary electrons in the electrostatic field is done using GPT [13].

In Figure 5 we show the electrostatic field and the SE tracing in the Faraday Cup for a -1000 V repeller. The voltage barrier in the axis of the FC is at ~200 V, allowing for SE recapture of less than ~200 eV. In the collector, the indentation acts as a voltage screen and the electric field is low. Since the electrons are emitted in the inclined faces (±60º), the electron recapture is mostly dominated by its arrival to the adjacent indentation face. Most SE are recaptured in times of less than a RF period of 2.84 ns (352.2 MHz), minimizing the interaction of SE with the next irradiation bunch. Only the electrons with energies higher than 100 eV can have long trajectories leading to longer recapture times, up to 5 ns.

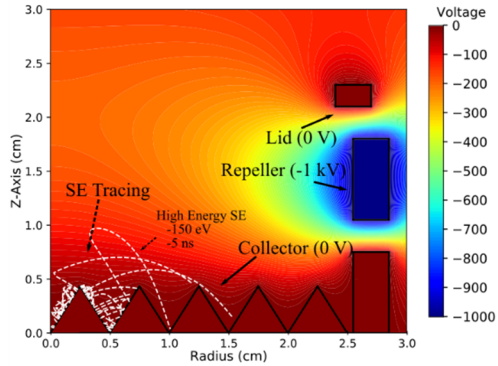

Figure 5: Voltage profile on the FC and secondary electron tracing (in dashed line).

In Figure 6 we show the fraction of escaping electrons as a function of the repeller voltage in the range of –1 kV to 1 kV. Full suppression is attained for repeller voltages up to -500 V. For repeller voltages of -500 V/-100 V a small fraction of high energy electrons (E_e>20 eV) escapes the Faraday Cup. For lower repeller voltages (-100 V/0 V), even low energy electrons could escape, and electron capture takes place only due to the indented geometry of the collector. Due to the 60º indented geometry half of the emitted electrons are captured at 0 V. For positive voltage, the repeller attracts the secondary electrons and the fraction of escaping electrons increases.

From the analysis of SE suppression, we offer an estimation of the performance of the MEBT FC. The model is simple and has some limitations: is based on the SE spectrum on carbon foils [12] and the influence of graphite surface finishing on the SE emission or other effects such as electron-electron or proton-electron interaction are not included. Even with some limitations the model allows to have an estimation of secondary electron recapture, and the effect of the geometry or the repeller voltage.

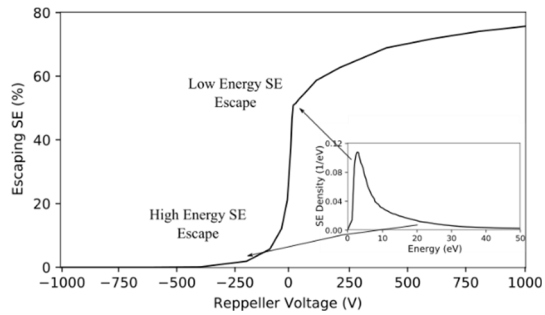

Figure 6: Fraction of SE escaping the FC as function of the repeller voltage. In the bottom-right corner the SE spectrum from Drexler et al. [12].

ESS-BILBAO INTEGRATION TEST

The Faraday Cup along with the control and electronics were integrated in the ESS-Bilbao Injector to check operation under beam conditions.

For the signal acquisition, a Front-End using active electronics has been developed by ESS-Bilbao. The Front-End converts and amplifies the collected current in the FC cup

ISBN: 978-3-95450-204-2 ISSN: 2673-5350 doi:10.18429/JACoW-IBIC2019-MOPP014

into a voltage signal with a gain of 100 V/A and a bandwidth of >2 MHz. For adequate signal conversion, the Front-End is placed in the MEBT, in the support structure near the FC. The Back-End contains the power supplies required by the system and the motion control and I/O signals are handled by Real-Time Beckhoff modules. The FC control system is integrated in a μTCA crate, where the signal control and acquisition is done by IOxOS boards, and the trigger synchronization is done by the MRF EVR-300U board. For the control integration, the different software layers are developed in the ESS EPICS Environment. EPICS published variables are monitored and controlled in an Engineering User Interface deployed in CS-Studio to be used in the FC commissioning stage.

The ESS-Bilbao Injector is composed by the Ion Source Hydrogen Positive (ISHP) and the Low Energy Beam Transport (LEBT) [14]. The extraction system allows for flexible beam conditions, in this case using energies of 45 kV, intensities of ~40 mA, pulse duration of 1.6 ms and repetition rates of 1 Hz. In the configuration used for these tests the LEBT includes three diagnostic boxes and a solenoid. The first box is equipped with an AC Current Transformer (ACCT1), then a solenoid is used for beam focusing, the second diagnostic box contains another ACCT2. During the tests the ACCT1 measured a maximum current of ~40 mA, and the ACCT2 currents of ~32 mA, meaning that the transmission in the solenoid is ~80%, which is the characteristic value of the ESS-Bilbao Injector. Finally, the FC is installed in a third diagnostic box, at ~600 mm distance from the ACCT2 and using a ϕ 25 mm collimating lid. The large beam size downstream the LEBT and the small aperture decrease the size of the beam collected in the FC signal compared to the ACCTs, down to ~5 mA.

In Figure 7 we show the signal in the FC for the different repeller voltages. The collected current increases in the first 0.5-1 ms up to a stable value, with currents of ~5 mA when the repeller is set at –1000 V. When the repeller voltage is set at 0 V the FC signal is biased by the escape of secondary electrons and the measured current is up to ~9 mA. Analysing the FC signal for different repeller voltages we observed saturation for values over -500 V, which agrees with the expected secondary electron suppression in the FC (see Figure 6). Since the recapture efficiency due to indentation is of 50% at 0 V, a secondary electron yield of Y_e~1.4 is estimated. From Mechbach et al. [15] yields of Y_e~3 are expected for 45 keV protons on carbon foils. The difference in the yields can be due to different aspects, such as the collector indented inclination, surface finishing, or different yield for graphite of carbon foils. It is important to underline that in the MEBT the SE yields will be much lower than in the tests at Bilbao, due to the lower stopping powers, ~160 MeV/cm at 3.63 MeV and ~1200 MeV/cm at 45 keV.

Finally, from the integration tests in ESS-Bilbao, some lessons were learned that allowed improvement of the acquisition system. A background noise was observed that we believe to be caused by different grounding of the beam line and acquisition system. Also, the Back-End was upgraded to allow operation with positive repeller voltages (up to +1000V).

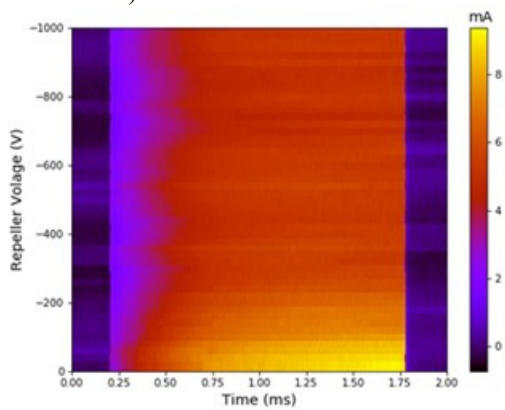

Figure 7: Signal read-out in the FC as function of time for different repeller voltages during the beam tests with the ESS-Bilbao injector.

CONCLUSIONS

In this work, we describe the design of the ESS MEBT FC and its integration test in the ESS-Bilbao ECR ion source.

The FC will operate under the MEBT commissioning modes measuring the beam current and as a beam stopper. For this purpose, a refrigerated cup using a graphite collector and a -1 kV repeller is designed. For the graphite collector, we study its thermo-mechanical response concluding that maximum temperatures and stresses in the irradiated graphite are lower than the design limits. For the secondary electron suppression, we study the electrostatic field and simulate the secondary electron production. We characterize the FC performance and obtain full suppression secondary electrons for voltages below -500 V.

Finally, we have integrated the FC and its electronics and control into the ESS-Bilbao injector, observing full SE suppression for repeller voltages below -500 V.

ACKNOWLEDGES

We would like to thank the BI and ICS groups of ESS for the collaboration in the development of the MEBT instrumentation, the mechanical department of ESS-Bilbao for the acceptance test and mechanical integration, to E. Artal of the U. Cantabria for the support on the manufacturing of Electronics and to F. Dubost and G. Gaubert of Pantechnik for the manufacturing of the Faraday Cup.

REFERENCES

[1] R. Garoby *et al.*, "The European Spallation Source Design," *Phys. Scr.*, vol. 93, no. 1, p. 014001, Jan. 2018.

[2] T. J. Shea *et al.*, "Overview and Status of Diagnostics for the ESS Project", in *Proc. IBIC'17*, Grand Rapids, MI, USA, Aug. 2017, pp. 8-15. doi:10.18429/JACoW-IBIC2017-MO2AB2

[3] R. Miyamoto, B. Cheymol, M. Eshraqi, and I. Bustinduy, "Beam Physics Design of the ESS Medium Energy Beam Transport", in *Proc. IPAC'14*, Dresden, Germany, Jun.

ISBN: 978-3-95450-204-2 ISSN: 2673-5350 doi:10.18429/JACoW-IBIC2019-MOPP014

2014, pp. 3326-3328. doi:10.18429/JACoW-IPAC2014-THPME045

[4] M. A. Plum *et al.*, "Beam Diagnostics in the SNS Linac," *AIP Conf. Proc.*, vol. 648, no. 1, pp. 195–202, Nov. 2002.

[5] D. B. Pelowitz, "MCNPX user's Manual Version 2.7.0," LA-CP-11-00438, Apr. 2011.

[6] "ANSYS - Simulation Driven Product Development." http://www.ansys.com

[7] SGL Group: The Carbon Company, "Specialty Graphites for the Metal Industry," https://www.sglcarbon.com

[8] D. Smith, W. Daenner, and Y. Gohar, "ITER blanket, shield and material data base," Oct. 1991.

[9] Y. Lee and M. Hartl, "ESS Target Materials Handbook," Internal ESS ESS-0028465, Feb. 2016.

[10] M. Bahrami, J. R. Culham, and M. M. Yovanovich, "Modeling Thermal Contact Resistance: A Scale Analysis Approach," *J. Heat Transf.*, vol. 126, no. 6, pp. 896–905, Jan. 2005.

[11] E. J. Sternglass, "Theory of secondary electron emission by high-speed ions," *Phys. Rev.*, vol. 108, no. 1, p. 1, 1957.

[12] C. G. Drexler and R. D. DuBois, "Energy-and angle-differential yields of electron emission from thin carbon foils after fast proton impact," *Phys. Rev. A*, vol. 53, no. 3, p. 1630, 1996.

[13] S. B. Van der Geer and M. J. De Loos, "General Particle Tracer: User Manual," User Manual Version 2.83.

[14] Z. Izaola et al., "Advances in the Development of the ESS-Bilbao Proton Injector," in *Proc. HB2016,* Malmö, Swed., 2016.

[15] W. Mechbach, G. Braunstein, and N. Arista, "Secondary-electron emission in the backward and forward directions from thin carbon foils traversed by 25-250 keV proton beams," *J. Phys. B At. Mol. Phys.*, vol. 8, no. 14, p. L344, 1975.